Thermal and electrical conductivity of approximately 100-nm permalloy, Ni, Co, Al, and Cu films and examination of the Wiedemann-Franz Law

A. D. Avery,[1,2] S. J. Mason,[1] D. Bassett,[1] D. Wesenberg,[1] and B. L. Zink[1]
[1]*Department of Physics and Astronomy, University of Denver, Denver, Colorado 80208, USA*
[2]*Department of Physics, Metropolitan State University of Denver, Denver, Colorado 80204, USA*
(Received 13 October 2014; revised manuscript received 10 September 2015; published 8 December 2015)

We present measurements of thermal and electrical conductivity of polycrystalline permalloy (Ni-Fe), aluminum, copper, cobalt, and nickel thin films with thickness <200 nm. A micromachined silicon-nitride membrane thermal-isolation platform allows measurements of both transport properties on a single film and an accurate probe of the Wiedemann–Franz (WF) law expected to relate the two. Through careful elimination of possible effects of surface scattering of phonons in the supporting membrane, we find excellent agreement with WF in a thin Ni-Fe film over nearly the entire temperature range from 77 to 325 K. All other materials studied here deviate somewhat from the WF prediction of electronic thermal conductivity with a Lorenz number, L, suppressed from the free-electron value by 10% to 20%. For Al and Cu we compare the results to predictions of the theoretical expression for the Lorenz number as a function of T. This comparison indicates two different types of deviation from expected behavior. In the Cu film, a higher than expected L at lower T indicates an additional thermal conduction mechanism, while at higher T lower than expected values suggests an additional inelastic scattering mechanism for electrons. We suggest the additional low-T L indicates a phonon contribution to thermal conductivity and consider increased electron-phonon scattering at grain boundaries or surfaces to explain the high-T reduction in L.

DOI: 10.1103/PhysRevB.92.214410 PACS number(s): 66.70.Df, 72.15.−v, 73.50.−h, 72.10.Di

I. INTRODUCTION

Recent studies of the interaction between heat, charge, and spin degrees of freedom in nanoscale magnetic systems have led to both interesting fundamental physics questions and highlighted potential new applications. This field of spincaloritronics [1–3] has also put a new emphasis on understanding the thermal and thermoelectric properties of magnetic thin films, particularly with thicknesses well into the <100-nm regime. Although charge transport in such samples is relatively straightforward to measure, measurements of heat flow for thin-film samples are typically made very difficult by the presence of the macroscopic heat sink of the bulk substrate that supports the film. This challenge has been addressed in recent years by several experimental advances and the study of heat transport at the nanoscale is expanding rapidly [4,5]. However, measurements of thermal conductivity, k, in very thin metal films remain difficult [6–8], and in light of this difficulty many authors make use of the Wiedemann–Franz (WF) law, $k_e/\sigma = LT$, to provide an estimate of the electronic thermal conductivity k_e by using measured values of electrical conductivity σ. This is used to estimate the total thermal conductivity k under the usually reasonable assumption that k_e is the dominant contribution. Here L is the Lorenz number, a material-dependent parameter usually assumed to have a constant value taken from the existing literature on bulk materials [9], or simply given by the Sommerfeld theory for free electrons, $L_o = \pi^2 k_b^2/(3e^2)$. However convenient, this "law" must be used with caution since even very pure bulk materials seemingly "violate" it as a function of temperature [10], and its validity for thin, polycrystalline metal films has never been clearly established [11–13].

In reality, the scattering rates of electrons in metals are often different for processes that affect charge transport and those that affect heat transport. Thorough examinations of WF for some complex, nanostructured, or thin-film materials indicate a more complicated picture of the WF law than often realized, ranging from a thickness-dependent violation in very early work on copper thin films [11], to agreement with WF in aluminum thin films [12], to excellent agreement with WF in granular bulk alloys [14], to deviations at high T for complex metallic alloys [15], to combined lattice-dynamic modeling and experimental probes that suggest decreased k_e and larger than expected phonon contributions, k_{ph}, even in bulk metals [16]. Existing investigations of thermal conductivity in single metallic nanowires suggest either excellent agreement with WF [17], or violations indicating the presence of a significant phonon thermal conductivity [18]. Measured values of thermal conductivity, particularly for transition-metal thin films, are essential for better understanding of a wide range of spintronic and spincaloritronic effects, including magneto-Seebeck effects in magnetic tunnel junctions [19–22], joule heating in nanowires [23], thermal spin torques [24–27], the longitudinal spin Seebeck effect [28–30], and spin-dependent Seebeck and Peltier effects [31,32].

In this paper we present direct measurements of both electrical and thermal conductivity on films of selected ferromagnetic and nonmagnetic metals with thickness $t <$ 200 nm. We control the thermal gradient applied to the films by using a suspended silicon-nitride (Si-N) membrane thermal-isolation platform. As shown in Fig. 1, this platform provides two large islands with lithographically patterned heaters and thermometers and a narrow bridge connecting them. This bridge is the sample growth platform, and in this study we deposited films on prefabricated and premeasured bridges through shadow masks. Further details of the fabrication and use of these platforms are available elsewhere [7,33]. Because the platform allows measurement of thermal conductance and electrical resistance on exactly the same thin-film sample

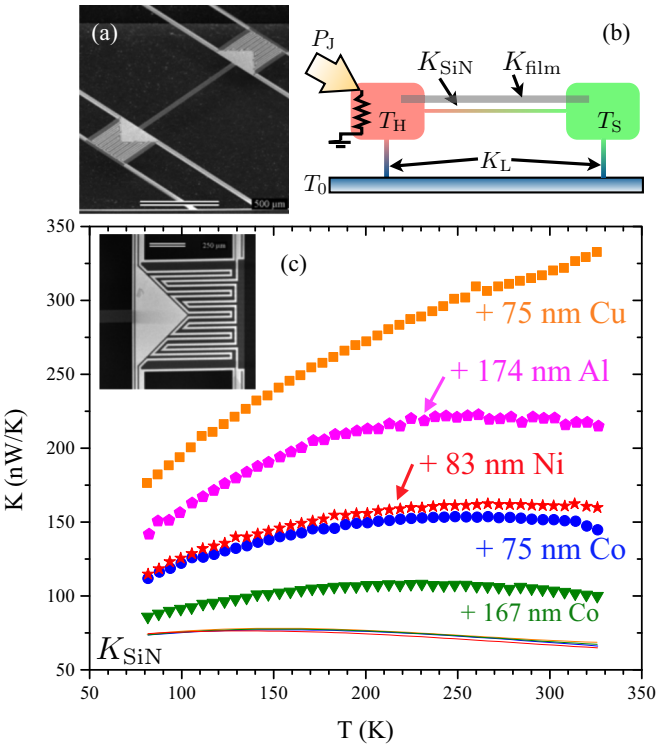

FIG. 1. (Color online) (a) Scanning electron micrograph shows a tilted view of the thermal-isolation platform including the narrow bridge used as a sample stage. (b) The thermal model used to analyze the response to heating power and to determine thermal conductances. (c) Total thermal conductance K vs average sample temperature T for single-component metal films compared to background K_{SiN}. All metal films dominate the thermal conductance, even at the lowest T. The inset shows a scanning electron micrograph of one island (here from the larger of the two platform sizes used in this work) that shows the electrical leads used to contact the film on the left, with the separate heater and thermometer metal strips visible at right along with the four leads used to measure each resistor.

and with the current and heat flow unambiguously in the same direction, many of the uncertainties in the transport coefficients are eliminated and the WF law can be tested very accurately. This is the main goal of the paper. An additional goal is to expand and revisit our earlier observation, made with similar thermal-isolation platforms, of a significantly reduced L for permalloy films for temperatures below ~175 K [34]. Such reductions in L are potentially very interesting in thermoelectric applications and warrant close examination.

We present a new study of the regime of apparent reduction in L for permalloys, which is very commonly used in spincaloritronic devices [31,32,35–40], making understanding of its thermal properties critical for the field. Here we take special care to avoid the possible effects of surface scattering of a surprisingly large population of long-wavelength phonons in the Si-N membrane that we have recently demonstrated [33]. The new results presented below agree with WF extremely well, and we demonstrate that the earlier reduction was most likely caused by surface-scattering effects in the background subtraction. For the higher-thermal-conductance films of Al, Cu, Co, and Ni, such background effects are not an issue due to the large difference between the background and film conductance values. All these films, including a Co film with a very large static defect density, show L reduced by up to 20% from typical literature values. Deviations in L at this level are not uncommon, but highlight that, in critical applications or where accurate tests of new theories of thermally driven spin effects are desirable, measurements of thermal conductivity are essential. In the case of Cu and Al we are able to further analyze $L(T)$ by comparisons to the theory for L based on electron-phonon and defect scattering in a metal with an essentially-free-electron-like Fermi surface [13,41]. This comparison not only supports the simple view of a reduced L, but actually suggests a low temperature enhancement in k for the Cu film. We consider a possible origin for this in a phonon thermal conductivity, an effect that has been seen in materials and nanostructures with reduced electronic thermal conductivities [16,18,42–46].

II. EXPERIMENT

Before continuing discussion of the experimental technique, we clarify our use of symbols. For thermal conductivity, the nominally intensive property with units of W/(m K), we use lower-case k. Without a subscript this indicates the total measured thermal conductivity of a film. Subscripts of k are used to indicate a contribution from a particular mechanism. We use upper-case K for the extensive property thermal conductance with units of W/K, with subscripts to indicate contribution from either certain parts of the measurement platform or the sample film.

We measured total thermal conductivity k, electrical resistivity $\rho = 1/\sigma$, and L by using suspended thermal-isolation platforms micromachined from 500-nm-thick silicon nitride (Si-N). The Si-N is amorphous and tuned away from the stoichiometric compound to achieve a low-stress film that survives removal of the bulk substrate. Two types of platforms were used in this work, both with identical geometry of the Si-N bridge and islands, but varying in fabrication technique and number of contacts to the films. Each platform is composed of either a 88×2050 μm^2 (Al) or 35×806 μm^2 (all other samples) bridge supported between two islands. Each island holds separate resistive heater and thermometers (with four-wire connections to each) as well as large triangular pads that provide electrical contacts to a sample film deposited on the bridge. All measurements are carried out in vacuum of 10^{-5} Torr or better, with the platform clamped to a radiation-shielded gold-plated high-conductivity copper sample mount. Thermometers are calibrated in each experimental run against a silicon diode reference thermometer mounted in the cryostat cold finger. The platforms used to measure Cu, Co, and Ni films have only two triangular pads to contact the sample film, though four wires are attached to these two contacts. This removes any contribution from lead resistance, but opens the possibility of a contact resistance between the sample film and the triangle leads contributing to the measured resistance. As discussed further below, we see little evidence that such a contact resistance contributes meaningfully to the measurement. The platform used to study the Al and the Ni-Fe film with 56-nm total thickness as described below have two additional leads to the sample region, allowing a true four-wire

electrical conductivity measurement of the sample film and removing this potential source of systematic error.

The thermal model that describes the platform is shown in Fig. 1(b). Heat flow through the thermal-isolation platform is confined to conduction only. The small area of the island on which the heating power is dissipated eliminates the radiation contribution typically problematic over 100 K in dc thermal measurements and vacuum eliminates convection. Assuming steady state and a small-signal limit, this model can be solved to yield

$$T_h = T_o + \left[\frac{(K_L + K_B)}{(2K_B + K_L)K_L}\right]P, \quad (1)$$

$$T_s = T_o + \left[\frac{K_B}{(2K_B + K_L)K_L}\right]P, \quad (2)$$

where K_B is the thermal conductance of the bridge, K_L the conductance of the supporting legs, P is the measured power dissipated in the sample heater, and T_h, T_s, and T_o are the temperature of the heated island, cooler island, and platform frame (and cryostat), respectively. Linear fits of measured T for a series of P values allow determination of K_B and K_L. In heat-transport measurements we limit the hot-island temperature to <20 K higher than T_o in this temperature range, which typically results in a difference across the sample of 5 K or less. When a film is deposited on the Si-N the total conductance of the link between the island has contributions from both the Si-N and the sample film so that $K_B = K_{\mathrm{SiN}} + K_{\mathrm{film}}$. We determine the contribution of a thin-film sample by first measuring K_B for the bare Si-N bridge, which gives K_{SiN} (as shown by solid lines in Fig. 1), and subtracting this background from K_B measured again after the film is deposited. These values of total conductance are much larger than K_{SiN} even for very thin metal films, as shown for Al, Cu, Ni, and Co. Thermal conductivity k for the film is determined from K_{film} via $k = K_{\mathrm{film}}l/(wt)$, where the lateral geometry is defined by the Si-N bridge, l and w, and the thickness of the sample, t, is determined via profilometry on a separate witness sample.

Resistance measurements of the sample deposited on the platform are straightforward and allow us to determine the Wiedemann–Franz ratio

$$L = \frac{k}{\sigma T} = \frac{K_{\mathrm{film}}R_{\mathrm{film}}}{T}. \quad (3)$$

Here the common sample geometry cancels, leaving only extensive transport properties. This removes the often dominant source of error from determination of L. Using the *total* thermal conductivity to determine L includes all thermal-transport mechanisms, such as phonon or magnon transport. These additional mechanisms cause increased values of L. As noted above, surface-scattering-induced modification of the Si-N background K_{SiN} can introduce systematic errors where K_{film} is small and no measures are taken to saturate the surface scattering [33]. We describe our methods to accomplish this saturation for the Ni-Fe experiment in more detail below.

All samples other than the Al film were deposited via e-beam evaporation through micromachined shadow masks onto the sample bridge in an ultrahigh-vacuum (UHV) chamber. Base pressures ranged between 4×10^{-10} and 1×10^{-8} Torr, with estimated growth pressure typically one order of magnitude higher, and a growth rate of ~0.1 nm/s. The Al film was grown via thermal evaporation in high vacuum ($\approx10^{-6}$ Torr) at a similar rate. Chamber pressure for the UHV system did not correlate strongly to properties of the deposited films with the exception of the two Co films. In this case the 167-nm film was grown at 0.1 nm/s after reaching base pressure of only 1×10^{-8} Torr, with growth pressures near 2×10^{-7} Torr. The thinner 75-nm film was grown after reaching 6×10^{-10} Torr at the same rate with growth pressures maintained at or below 2×10^{-8} Torr. This clearly affected the quality and transport properties of these two films. Permalloy films were grown from pre-alloyed material (nominal composition $Ni_{80}Fe_{15}Mo_5$) from a single crucible. Al, Cu, Ni, and Co starting source materials were of 99.999%, 99.999%, 99.995%, and 99.95% nominal purity, respectively. Thickness was measured via atomic force microscopy (AFM) profilometry on witness substrates mounted on a rotating sample plate in the same deposition as the thermal-isolation platforms.

III. RESULTS

Figures 2(a)–2(c) shows ρ, k, and L, respectively, measured for Al, Cu, Ni, and two Co films. Note the break in the axis in Fig. 2(a) and the very high ρ for the thicker Co film. As noted in Sec. II, this film was grown in far-from-ideal UHV conditions and contains a large number of static defects. ρ for the other films shows expected behavior, with larger values than reported for bulk, but following trends in bulk values with Ni and Co nearly equal and Cu much lower. Figure 2(b) shows k measured (as determined from the K data of Fig. 1 and measured film geometry) for the exact same films as in Fig. 2(a). Although studies of k for thin metal films with thickness near 100 nm are rare, an existing study of Cu films showed values ranging from 80 to 300 W/(m K) over a similar T range for films near 100 nm but with lower values of ρ [11]. This is quite consistent with our results. Figure 2(c) shows our experimental Lorenz number $L = K_{\mathrm{film}}R_{\mathrm{film}}/T$. Again, note that because the measurements are performed on the exact same film, neither the in-plane width and length nor the sample-film thickness affects this measurement. Therefore uncertainty in this geometry, often the dominant source of error in transport measurements, does not directly affect L. Here the free-electron Sommerfeld value L_o is also shown (dashed line). All five films, including the higher ρ Co film, show similar values and behavior with T, and all are depressed from L_o. We consider possible physical mechanisms for such a suppression below. Note that presence of a contact resistance in the R measurement (only a possibility for the Co, Cu, and Ni films) would cause a higher L, via the higher apparent R. This is clearly not the case here. Furthermore, since ρ values are in line with expectations for films of this quality and thickness, a large contact resistance is unlikely.

Figure 3 describes results of two in-depth experiments aimed at eliminating surface-scattering-induced background changes and determining a more accurate value of k for permalloy thin films. In both we use a thin layer of Ni-Fe to saturate the surface scattering in the Si-N membrane, then continue to deposit and measure thicker Ni-Fe films and calculate K_{film} using this "saturated" background. This method

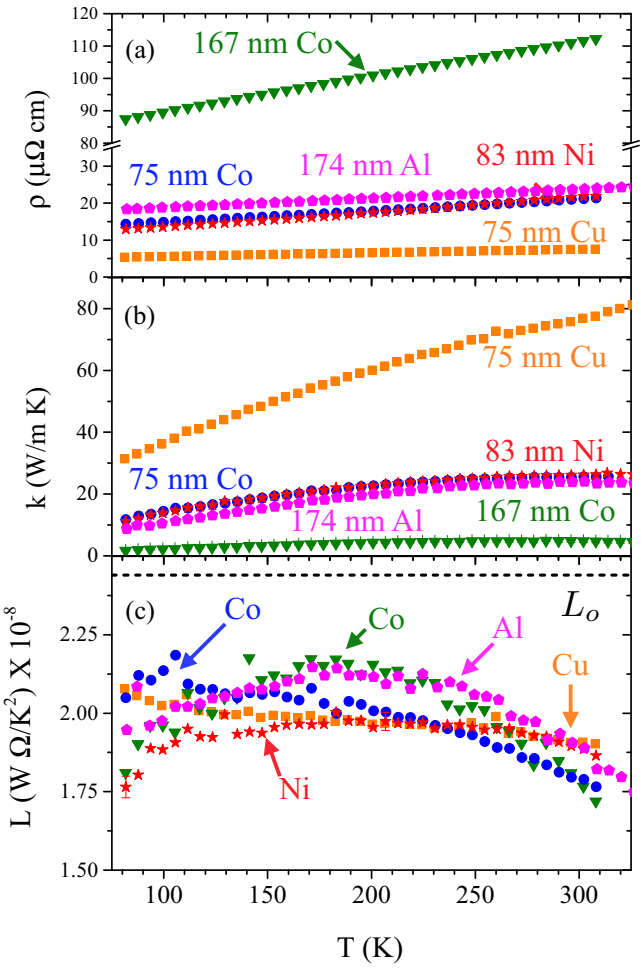

FIG. 2. (Color online) Electrical and thermal transport as a function of T for single-component films. (a) ρ vs T. The thicker Co shows very high resistivity as a result of poor growth conditions. (b) Thermal conductivity k vs T showing the same trends. (c) Lorenz ratio kT/σ shows very similar values across all films, with all suppressed from the free-electron Sommerfeld value L_o shown by the dashed line. Estimated combined statistical and systematic error on L is 2×10^{-10} WΩ/K^2 or better.

follows from similarly detailed studies of surface-scattering induced by thin, discontinuous Au films and is described in detail elsewhere [33]. Experiments shown in both Figs. 3(a) and 3(b) start with a measurement of the bare Si-N. In each experiment we then deposited 4 nm of Ni-Fe on the Si-N bridge. In Fig. 3(a), and as shown schematically in cross section in Figs. 3(c) and 3(e), this film and all subsequent films were deposited with "shadow mask B" (SM B), which protects the area outside the dotted line in the inset schematic, and allows the film to contact the leads on each island that provide electrical contact to the sample. Since the initial 4-nm Py was uncapped in order to prevent confusing the results by adding thin layers of other materials, this film oxidized even in the short time (~30 to 60 min) required to remove it from the deposition chamber and install it in the cryostat. The effect of this oxide seems minimal for thermal conductivity experiments, where the existence of parallel heat-conduction paths is the most important criterion for the measurement. However, as depicted in Fig. 3(e), the oxide was thick enough to prevent Ohmic contact with the subsequent film layers, and we found R measurements of this sample impossibly unreliable.

To prevent this oxidization but still allow saturation of the phonon surface scattering in the Si-N bridge, we deposited the 4-nm layer for the experiment shown in Fig. 3(b) through a smaller shadow mask, "shadow mask A" (SM A) as shown in Fig. 3(d), that left the leads to the sample free of Py. With existing equipment we cannot prevent the exposure of the sample to air, but by preventing the contact of the first 4-nm Py layer with the leads, the subsequent 52-nm film [deposited again using SM B as shown in Fig. 3(f)] makes Ohmic contact with the leads and gives reliable R measurements. The resulting film resistivity is ~27 $\mu\Omega$ cm at room temperature, a factor of two or more lower than our earlier Ni-Fe films [34], and in line with typical values for good quality permalloy of this thickness.

Figure 4(a) shows the k values determined from $K_{\rm film}$ values determined from data in Figs. 3(a) and 3(b). The k values for all films are tightly grouped, with a roughly linear T dependence expected from $k_{\rm e} = 1/(3c_{\rm el}v_{\rm F}\ell_{\rm e}) = 1/(3\gamma T v_{\rm F}\ell)$ for electronic thermal conductivity in the limit of a temperature-independent electron mean-free path, $\ell_{\rm e}$. γ is the electronic heat capacity coefficient and $v_{\rm F}$ is the Fermi velocity. Here we also compare our k data for Ni-Fe films from an earlier paper [34]. Note that these curves are less linear, and that the drop at lower T is the feature that drives the drop in L we previously reported. This is obvious in Fig. 4(b), where the L values drop starting at ~200 K. The curves in both panels labeled "estimated $K_{\rm SiN}$" are described further below. Figure 4(b) also shows results for the 56-nm film, where we have eliminated surface-scattering effects, which are an issue for Ni-Fe since values of $K_{\rm film}$ for the alloy are much smaller than for the elemental metal films. The experiment presented in Figs. 3 and 4 represents the most careful examination we have performed of transport in Ni-Fe. Here we see excellent agreement with L_o for nearly the entire T range of the experiment, as often seen in alloys due to additional elastic electron scattering with disorder [14,47], with only a small peak at lower temperatures, which is discussed in more detail below (Sec. IV).

In Fig. 5 we estimate if the type of drop in $K_{\rm SiN}$ caused by addition of a film to the Si-N bridge and so clearly visible in Figs. 3(a) and 3(b) could explain the drop in L below 200 K reported in our earlier work. In this plot of thermal conductance, we compare the measured background $K_{\rm SiN}$ for the 2010 data with the more recent measurement from Fig. 3(a). These two platforms were fabricated by using the same techniques and materials, and indeed show nearly exact agreement of the background thermal conductance before addition of any film. If we assume that addition of a film reduced the Si-N background by the same amount as in the recent measurement, we can make an estimate of the actual k for this film by subtracting the saturated background (shown as a solid line). The resulting values of $K_{\rm film}$ and k are shown in Figs. 4(a)–4(b) and labeled "using estimated $K_{\rm SiN}$." This curve both recovers the nearly linear k vs T shown in the other Ni-Fe films and shows the same excellent agreement with WF. The overall magnitude of k for these films remains low due again to poorer growth conditions.

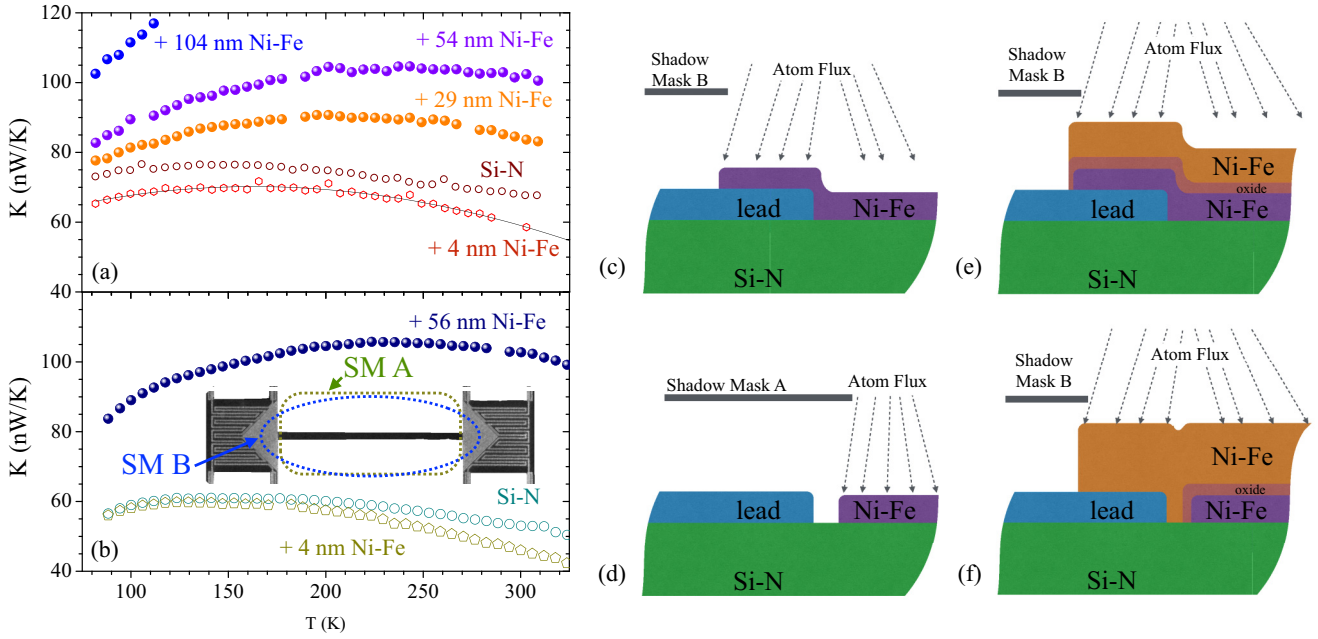

FIG. 3. (Color online) Total thermal conductance K for two platforms used to study Ni-Fe. In panel (a), measurements of successive depositions of Ni-Fe are shown, building eventually to a total thickness of ≈100 nm (this platform failed near 120 K, preventing further data for the thickest film). Note that deposition of a very thin, poor-conductance, 4-nm-thick layer actually *reduces* the total thermal conductance of the bridge. We have previously shown this to be due to modification of surface scattering at the Si-N/film surface and that the effect "saturates" after addition of even a few nm of metal film [33]. The solid line shows the saturated background conductance subtracted from the remaining data to determine k shown in Fig. 4(a). In panel (b), a single 52-nm-thick layer was deposited after the addition of a 4-nm-thick "saturating" film. The inset schematically shows that this saturating film was deposited through a smaller shadow mask, labeled "SM A" in order to avoid coating the electrical leads to allow reliable R and L measurements for Ni-Fe. The shadow mask process for the two different experiments is shown in schematic cross-sectional views in panels (c)–(f) as described in the text.

IV. DISCUSSION

Figure 6 shows the estimated conduction electron mean-free path, ℓ_e, determined from the measured k using $k = 1/(3c_{el}v_F\ell_e)$ with $c_{el} = \gamma T$ being the electronic specific heat and v_F being the Fermi velocity. Here we have used measured values of v_F [48], and γ [49]. These can deviate strongly from the simple free-electron model for transition metals and especially for the magnetic $3d$ atoms. In all cases $\ell \ll t_{film}$ and in the thicker, highly resistive Co film approaches the average interatomic distance. The short mean-free paths suggest that films in this regime of impurities (typical for vapor-deposited polycrystalline films common in devices and industrial applications) are not strongly affected by classical-size effects such as described by the Fuchs–Sondheimer, Mayadas–Shatkes, or similar models [50–52] and that our values of k and L should provide more reliable estimates than use of the WF law with the Sommerfeld value for such films.

For a more in-depth examination of the WF law we must consider the well-known temperature dependence of L. The theoretical expression for the Lorenz ratio, $L_{Th}(T)/L_0$, as a function of temperature that takes into account electron-phonon and impurity scattering is given by [13,41]

$$\frac{L_{Th}(T)}{L_0} = \frac{\frac{R_0}{R_{e-ph}} + \left(\frac{T}{\theta_D}\right)^5 J_5\left(\frac{\theta_D}{T}\right)}{\frac{R_0}{R_{e-ph}} + \left(\frac{T}{\theta_D}\right)^5 J_5\left(\frac{\theta_D}{T}\right)\left[1 + \frac{3}{\pi^2}\left(\frac{k_F}{q_D}\right)^2\left(\frac{\theta_D}{T}\right)^2 - \frac{1}{2\pi^2}\frac{J_7\left(\frac{\theta_D}{T}\right)}{J_5\left(\frac{\theta_D}{T}\right)}\right]}. \quad (4)$$

Here k_F is the Fermi wave vector, θ_D and q_D are the Debye temperature and wave vector, respectively, and

$$J_n\left(\frac{\theta_D}{T}\right) = \int_0^{\theta_D/T} \frac{x^n e^x}{(e^x - 1)^2} dx. \quad (5)$$

The ratio $R_0/R_{e\text{-}ph}$ quantifies the level of impurity scattering, where R_0 is the residual resistance and $R_{e\text{-}ph}$ is the contribution from electron-phonon scattering. Although this expression involves a number of assumptions including considering only spherical Fermi surfaces, equilibrium phonon distributions, and N-processes for electron-phonon scattering, it has been used to help understand potentially complicated metallic nanostructures [17]. For the metals studied here its use is most reasonable for Cu, which has the most nearly spherical Fermi surface. We also perform the calculation for Al, although we use the result only qualitatively. The expression should not be expected to predict behavior for the more complicated, spin-dependent Fermi surfaces of Co and Ni.

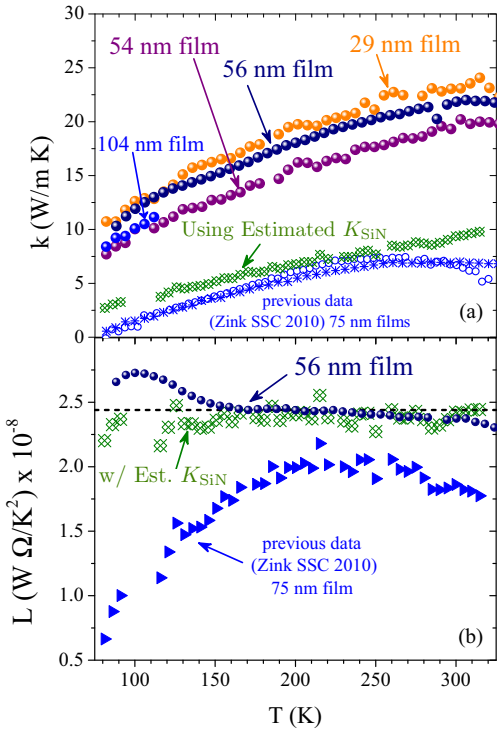

FIG. 4. (Color online) (a) k vs T determined from K shown in Fig. 3. All values show rough agreement and approximately linear k. (b) L values for Ni-Fe, comparing our best measurement with previously published values. Again, estimated total statistical and systematic error on L is 2×10^{-10} WΩ/K^2 or better. By using an estimate of the surface-scattering effect on the background K_{SiN}, we show that the previous data are in line with higher L with no strong temperature dependence.

In Fig. 7 we compare calculations using Eq. (4) to measured $L(T)/L_0$ for Cu and Al films. Here, bottom axes are T/θ_D using the high T values $\theta_{D,Cu} = 315$ K [53] and $\theta_{D,Al} = 390$ K

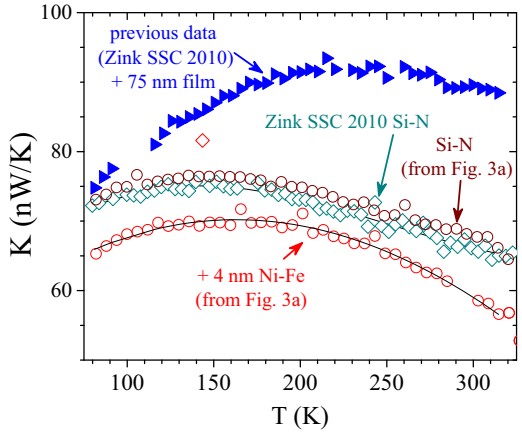

FIG. 5. (Color online) In-depth estimation of surface-scattering effects in background K_{SiN} for low-thermal-conductance Ni-Fe films. Open symbols show the background measurements for previous and current work. Both of these platforms were fabricated with the same geometry from similar starting wafers and materials and had very similar original values of K_{SiN}.

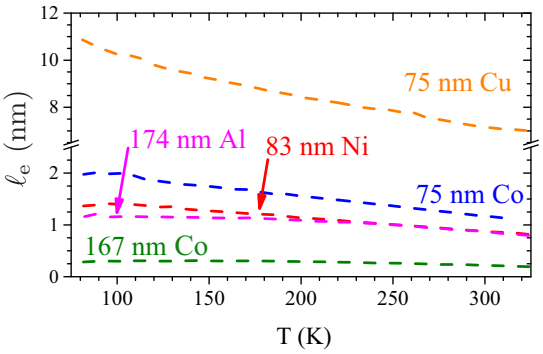

FIG. 6. (Color online) Estimated electron mean-free path, ℓ_e vs T for Al, Cu, Co, and Ni films determined from the kinetic expression for k using electronic heat capacity with bulk γ. An estimate for Ni-Fe is not shown due to lack of information on the electronic heat capacity, but should also be on the order of nm or below. All values are short compared to t_{film}.

[54]. $q_D = \theta_D k_b/(\hbar v_s)$ is calculated by using a weighted average of the transverse and longitudinal sound velocities for each metal for v_s. Heavy lines show the calculation using only the ideal (e-ph scattering) electrical and thermal resistances, and indicate the drop in L caused by the dominance of inelastic, vertical scattering of electrons by phonons in the regime where $T < \theta_D$. Broken lines show the calculation using values for $R_0/R_{e\text{-}ph}$ determined for our films. Calculation of $R_{e\text{-}ph}$ from first-principles requires knowledge of the electron-phonon coupling constant and therefore detailed understanding of the phonon spectrum that is not available for our films. An estimate of $R_0/R_{e\text{-}ph} = \rho_0/\rho_{e\text{-}ph}$ that is appropriate for the range of T discussed here where ρ remains linear with T to a very good approximation, which for metals often persists to lower T than suggested by typical Bloch–Gruneisen theory [17,55,56], can be made by using the expression $\rho_{e\text{-}ph} = AT/(4\theta_D)$ so that $d\rho/dT = A/(4\theta_D)$ [13,17]. Residual resistivity was taken either from measurements of the film resistivity to 5 K [for Cu, see inset to Fig. 7(a)] or estimates based on the deviation of higher-T data from bulk values assuming Matthiesen's rule (for Al). Although these calculations do make simplifying assumptions, they are the best possible representation of $L_{Th}(T)$ for these relatively simple metals. Note that, to calculate $R_0/R_{e\text{-}ph}$, we used $d\rho/dT$ taken from bulk ρ data, rather than that for the sample films. Both approaches lead to very similar values of $L_{Th}(T)$ and use of the film values would further lower the theory curve, leading to somewhat larger positive deviations of the experimental data from the theory.

In both Figs. 7(a) and 7(b) we see somewhat lower values of $L(T)/L_0$ near room temperature, in agreement with the very simple view of L shown in Fig. 2(c). However, at lower temperatures the Al film matches theory predictions extremely well, while the Cu film has a large *positive* deviation from expected behavior. This could be driven by a breakdown of the theory due, for example, to dominance of either the electron states in the nonspherical "neck" portions of the Cu Fermi surface, or of Umklapp scattering (U-processes) over the normal scattering assumed in the theory. However, this positive deviation from the expected $L_{Th}(T)/L_0$ could also be taken as evidence of a phonon contribution to thermal conductivity,

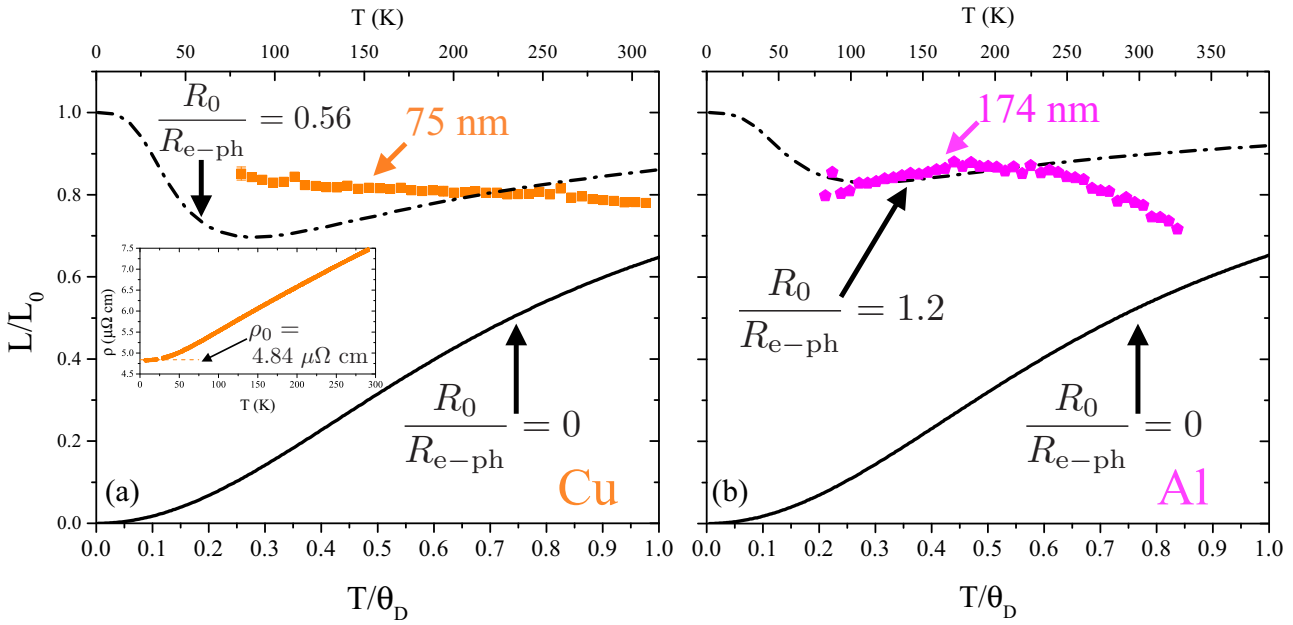

FIG. 7. (Color online) Closer examination of the temperature dependence of L for Cu and Al. The ratio $L(T)/L_o$ is plotted vs T/θ_D (with T shown on the top axis). Data points represent measured $L(T)/L_o$ for (a) Cu and (b) Al films. Lines are theoretical predictions of Eq. (4), with the solid line showing $L(T)/L_o$ for an ideally pure material and the broken line using a resistivity ratio matched to that measured for each film. Inset to (a) shows the measured electrical resistivity of the Cu film down to 5 K and the value of the residual resistivity ρ_0.

k_{ph}. Phonon contributions have been observed in nanoscale metal structures, typically when large defect density or other static disorder reduce the electronic thermal conductivity, k_e, strongly [18,43–46]. Such a phonon contribution leads to a total film thermal conductivity $k = k_e + k_{ph}$ so that the measured Lorenz number in this regime becomes

$$L = \frac{(K_e + K_{ph})R_{film}}{T} = L_{Th}(T) + \frac{K_{ph}R_{film}}{T}, \qquad (6)$$

and k_{ph} is given by

$$k_{ph} = \frac{[L(T) - L_{Th}(T)]T}{\rho}, \qquad (7)$$

where L_{Th} is taken from Eq. (4), $L(T)$ is the measured Lorenz number [Eq. (3)], and ρ is the measured film electrical resistivity.

The resulting estimate for k_{ph} for the Cu film below 225 K is shown in Fig. 8(a). Also shown is the calculated Debye (phonon) contribution to heat capacity, C_D, for $\theta_D = 315$ K. This is used in the kinetic expression $k_{ph} = 1/(3C_D v_s \ell_{ph})$ to estimate the phonon mean-free path, ℓ_{ph}, as shown in Fig. 8(b). As expected for a disordered material and in this temperature range where a large population of both phonons and electrons are available for scattering, ℓ_{ph} remains very short and is increasing as T drops. Although phonon thermal conductivity has been studied in some detail for bulk copper at helium temperatures [47,57–59], where impurity scattering dominates transport and the WF clearly holds, allowing confident determination of k_e, there are very few experimental studies of k_{ph} for bulk Cu at higher T, and none for Cu thin films to our knowledge. However, the estimated size of k_{ph} for this thin polycrystalline film is about half that expected from simple theory for pure bulk Cu at these temperatures (∼5 to 15 W/(m K)) [47], and is also comparable to that seen in bulk Cu alloys (≈8 W/(m K) at 80 K which is the highest T studied) [60]. We plan further study at lower temperatures

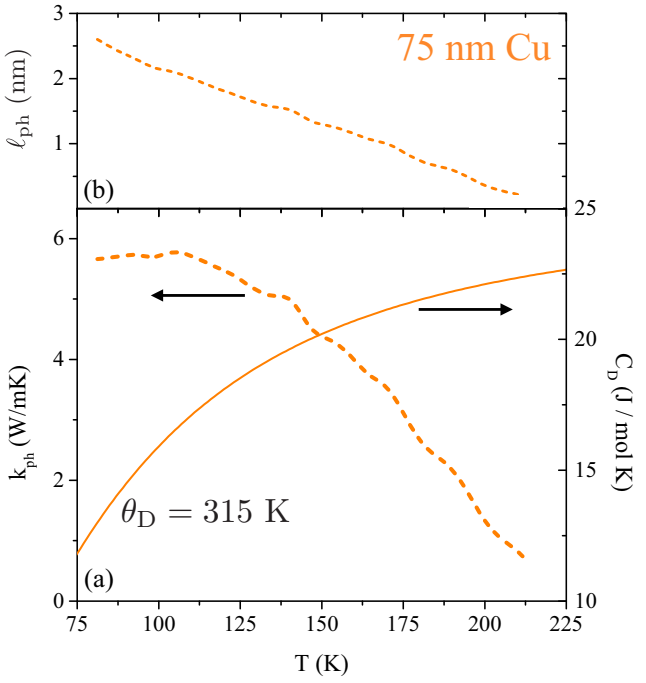

FIG. 8. (Color online) (a) The left axis shows estimated phonon contribution to k in the 75-nm Cu film below 225 K, calculated from the values of $L(T)/L_0$ in excess of the theory curve over this range of T as described in the main text. The right axis shows the Debye (phonon) heat capacity calculated for Cu, which is used in estimation of the phonon mean-free path, ℓ_{Ph} that is shown in (b).

and of a broader range of films to help clarify if this is truly a phonon contribution.

At higher temperatures both Al and Cu films show an effect opposite to an additional conduction pathway, with $L(T) < L_{\rm Th}(T)$. This violation of WF suggests additional scattering that relaxes the temperature distribution more effectively than the potential distribution. We investigate the length scale of this scattering event again by reference to the theory of Eq. (4). Here we assume Matthiessen's rule holds for the scattering time for thermal relaxation so that

$$\tau_{k,\rm tot} = \left(\frac{1}{\tau_{k,\rm Th}} + \frac{1}{\tau_{k,\rm vio}}\right)^{-1}. \tag{8}$$

Here $\tau_{k,\rm Th}$ is the scattering time including e-ph and impurity scattering underpinning Eq. (4) and $\tau_{k,\rm vio}$ is the scattering time for the additional inelastic scattering that drives the WF violation. The typical derivation of the WF law uses expressions for σ and $k_{\rm e}$ from the Drude model, kinetic theory, and the nearly-free-electron assumption,

$$\sigma = \frac{ne^2\tau_\sigma}{m^*}, \tag{9}$$

and

$$k_{\rm e} = \frac{1}{3}c_{\rm e}v_{\rm F}^2\tau_k = \frac{1}{6}n\pi^2k_B^2\frac{T}{E_{\rm F}}v_{\rm F}^2\tau_k, \tag{10}$$

where we write distinct time constants for electrical and thermal relaxation processes. The ratio of $k_{\rm e}$ to σ is then

$$\frac{k_{\rm e}}{\sigma} = \frac{\pi^2}{3}\frac{k_B^2}{e^2}\frac{\tau_k}{\tau_\sigma}T = L_0\frac{\tau_k}{\tau_\sigma}T, \tag{11}$$

so that

$$L(T) = \frac{k_{\rm e}}{\sigma T} = L_0\frac{\tau_k}{\tau_\sigma}. \tag{12}$$

When the two scattering times are equal, the familiar WF law results. When these do not cancel, the ratio $L(T)/L_0$, with $L(T)$ taken from the measured transport, is also the ratio of the total thermal and electrical scattering times, $L(T)/L_0 = \tau_{k,\rm tot}/\tau_\sigma$. When deviations from L_0 are only from the processes considered in the theory of Eq. (4), we then have $L_{\rm Th}(T)/L_0 = \tau_{k,\rm Th}/\tau_\sigma$. Using this we write

$$\tau_{k,\rm tot} = \left(\frac{L_0}{L_{\rm Th}(T)\tau_\sigma} + \frac{1}{\tau_{k,\rm vio}}\right)^{-1}. \tag{13}$$

Here $\tau_\sigma = m^*/(\rho ne^2)$ and $\tau_{k,\rm tot} = 3k/(\gamma T v_{\rm F}^2)$ are calculated for Cu by using measured ρ and electron density $n_{\rm Cu} = 8.49\times10^{28}$ m^{-3}. The resulting calculation for $\tau_{k,\rm vio}$ (right axis) vs T above 225 K, with the mean-free path $\ell_{\rm vio} = \tau_{k,\rm vio}v_{\rm F}$ (left axis) also shown, appears in Fig. 9. The result indicates a fairly strong T dependence and quite long length scales (up to 1 μm) for the inelastic, small-angle scattering events that cool electrons without strongly affecting their momentum. It also intriguingly seems to saturate very near the length scale of the film thickness (75 nm) at the highest T. This suggests that the additional inelastic scattering not only involves phonons but is also associated either with the film surfaces or grain boundaries, since grains in this evaporated film are expected to have lateral dimensions on the order of the film thickness.

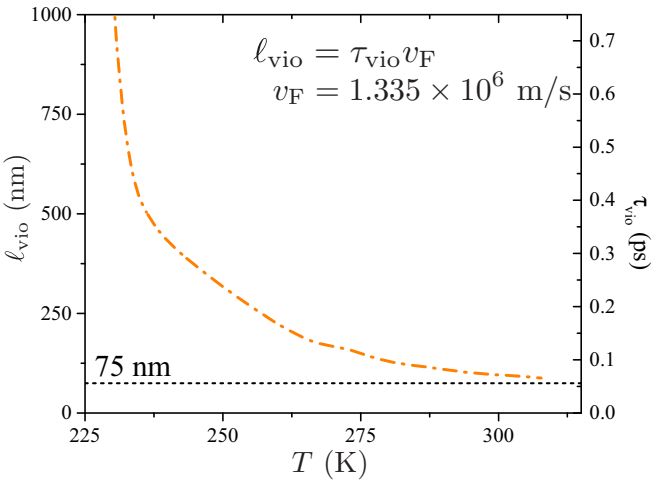

FIG. 9. (Color online) Estimated *electron* mean-free path (left axis) and scattering time (right axis) for the inelastic, small-angle scattering process present in the Cu film that violates the WF law at high T. The apparent saturation of the average distance between scattering events at a length comparable to the film thickness, and therefore to the grain size, at the highest T implies an origin in phonon-assisted inelastic grain-boundary scattering.

The overall picture of electron scattering in this film is that most electrons experience elastic, large-angle scattering, presumably from impurities, that result in mean-free paths on the short length scale shown in Fig. 6. However, some small fraction of electrons travel longer distances on average while experiencing inelastic scattering events involving phonons at grain boundaries, where they lose energy, cooling the electrons.

We have also considered an origin of this reduced $k_{\rm e}$ near room temperature related to an overall softening of the phonon density of states, which has in some cases been observed for thin films or nanoscale samples [61–65]. Such a shift could reduce the probability of the large-angle phonon scattering events required to return $L(T)$ to the Sommerfeld value at high T, thereby requiring higher temperatures to finally reenter the WF regime. However, our calculations suggest that the shifts in the phonon density of states (DOS) required to explain the ~20% reduction in L seen here are so large that they would drive deviations of the heat capacity away from bulk-like values, in contrast to experimental data showing very good agreement between bulk and even very thin Au and Cu films [66]. We are currently beginning a more detailed study of effects in Au and Cu films in order to clarify the physics of this additional scattering.

Finally, we offer a brief comment on the low-temperature upturn in the 56-nm Ni-Fe L data [Fig. 4(b)]. As discussed above, values of $L > L_o$ indicate a larger k than expected for a given σ by the WF law and can occur via additional mechanisms for thermal conduction such as phonons or magnons that are normally small contributions compared to electron thermal conductivity in metals. Note that the peak is also clearly visible in k for this film [Fig. 4(a)] such that the origin of the peak is entirely in additional thermal conductivity. However, this feature is absent in earlier (less-well-controlled) Py films. We found relatively little prior work on thermal

conductivity of permalloys or other Ni-Fe alloys in this regime of T. Existing studies do show peaks in thermal conductivity for a range of alloys [67,68], and in one case an upturn in L below ~200 K [68]. Moore *et al.*, suggest that a lattice (phonon) thermal conductivity is involved in their k peak and is the source of the upturn in L. It is possible to crudely explain the magnitude, if not the exact temperature dependence, of the peak in the 56-nm Py k with either a phonon or magnon contribution. Since the current data support little meaningful physical insight on this possible contribution, we leave attempts at quantitative analysis to future studies.

V. CONCLUSIONS

In summary, we presented measurements of k, ρ, and L for a series of metal films with thickness <200 nm. Films of Al, Cu, Ni, and Co all show somewhat reduced k from the simple expectation of the WF law throughout our 77 to 325 K temperature range, but approximate agreement with WF when using a reduced value of L. A careful examination of k and L in a permalloy film, using special techniques to eliminate a reduction of the background thermal conductance caused by surface scattering of phonons, shows that the permalloy obeys the WF well with no drop at low T. Estimates of the electron mean-free path in these films based on measured k suggest that all measurements are in the regime where film thickness $t_{\text{film}} > \ell_e$, which should make these values of L applicable for many studies of spincaloritronic and thermoelectric devices constructed of polycrystalline films with similar preparation and quality. A detailed examination of the temperature-dependence of L for Cu and Al films using the known theory reveals "violations" of WF at both low and high T and suggests the possibility of a phonon contribution to thermal conductivity at low T in the Cu film, and phonon-assisted grain-boundary or surface scattering at higher T. These results highlight the importance of both continued experimental and theoretical work to understand the temperature dependence of the Lorenz number and physics of thermal conductivity in metal thin films.

ACKNOWLEDGMENTS

We thank R. Sultan and A. Hojem for helpful discussions and assistance in the lab, and gratefully acknowledge support from the NSF (DMR-0847796 and DMR-1410247). This work was performed, in part, at the Center for Integrated Nanotechnologies, an Office of Science User Facility operated for the U.S. Department of Energy (DOE) Office of Science by Los Alamos National Laboratory (Contract DE-AC52-06NA25396) and Sandia National Laboratories (Contract DE-AC04-94AL85000).

[1] S. R. Boona, R. C. Myers, and J. P. Heremans, Energy Environ. Sci. **7**, 885 (2014).
[2] G. E. W. Bauer, E. Saitoh, and B. J. van Wees, Nat. Mater. **11**, 391 (2012).
[3] G. E. W. Bauer, A. H. MacDonald, and S. Maekawa, Solid State Commun. **150**, 459 (2010).
[4] D. G. Cahill, P. V. Braun, G. Chen, D. R. Clarke, S. Fan, K. E. Goodson, P. Keblinski, W. P. King, G. D. Mahan, A. Majumdar, H. J. Maris, S. R. Phillpot, E. Pop, and L. Shi, Appl. Phys. Rev. **1**, 011305 (2014).
[5] D. G. Cahill, W. K. Ford, K. E. Goodson, G. D. Mahan, A. Majumdar, H. J. Maris, R. Merlin, and S. R. Phillpot, J. Appl. Phys. **93**, 793 (2003).
[6] F. Volklein, H. Reith, and A. Meier, Phys. Status Solidi A **210**, 106 (2013).
[7] R. Sultan, A. D. Avery, G. Stiehl, and B. L. Zink, J. Appl. Phys. **105**, 043501 (2009).
[8] B. L. Zink, B. Revaz, J. J. Cherry, and F. Hellman, Rev. Sci. Instrum. **76**, 024901 (2005).
[9] G. S. Kumar, G. Prasad, and R. O. Pohl, J. Mater. Sci. **28**, 4261 (1993).
[10] J. G. Hust and L. L. Sparks, NBS Technical Note 634 (1973).
[11] P. Nath and K. Chopra, Thin Solid Films **20**, 53 (1974).
[12] T. Starz, U. Schmidt, and F. Volklein, Sensor. Mater. **7**, 395 (1995).
[13] T. M. Tritt, *Thermal Conductivity* (Kluwer, New York, 2004).
[14] L. Piraux, M. Cassart, J. S. Jiang, J. Q. Xiao, and C. L. Chien, Phys. Rev. B **48**, 638 (1993).
[15] E. Maciá, Phys. Rev. B **79**, 245112 (2009).
[16] X. Zheng, D. Cahill, P. Krasnochtchekov, R. Averback, and J.-C. Zhao, Acta Mater. **55**, 5177 (2007).
[17] D. Kojda, R. Mitdank, M. Handwerg, A. Mogilatenko, M. Albrecht, Z. Wang, J. Ruhhammer, M. Kroener, P. Woias, and S. F. Fischer, Phys. Rev. B **91**, 024302 (2015).
[18] M. N. Ou, T. J. Yang, S. R. Harutyunyan, Y. Y. Chen, C. D. Chen, and S. J. Lai, Appl. Phys. Lett. **92**, 063101 (2008).
[19] A. Boehnke, M. Walter, N. Roschewsky, T. Eggebrecht, V. Drewello, K. Rott, M. Munzenberg, A. Thomas, and G. Reiss, Rev. Sci. Instrum. **84**, 063905 (2013).
[20] N. Liebing, S. Serrano-Guisan, P. Krzysteczko, K. Rott, G. Reiss, J. Langer, B. Ocker, and H. W. Schumacher, Appl. Phys. Lett. **102**, 242413 (2013).
[21] N. Liebing, S. Serrano-Guisan, K. Rott, G. Reiss, J. Langer, B. Ocker, and H. W. Schumacher, Phys. Rev. Lett. **107**, 177201 (2011).
[22] M. Walter, J. Walowski, V. Zbarsky, M. Munzenberg, M. Schafers, D. Ebke, G. Reiss, A. Thomas, P. Peretzki, M. Seibt, J. S. Moodera, M. Czerner, M. Bachmann, and C. Heiliger, Nat. Mater. **10**, 742 (2011).
[23] H. Fangohr, D. S. Chernyshenko, M. Franchin, T. Fischbacher, and G. Meier, Phys. Rev. B **84**, 054437 (2011).
[24] J. Flipse, F. K. Dejene, and B. J. van Wees, Phys. Rev. B **90**, 104411 (2014).
[25] W. Jiang, P. Upadhyaya, Y. Fan, J. Zhao, M. Wang, L.-T. Chang, M. Lang, K. L. Wong, M. Lewis, Y.-T. Lin, J. Tang, S. Cherepov, X. Zhou, Y. Tserkovnyak, R. N. Schwartz, and K. L. Wang, Phys. Rev. Lett. **110**, 177202 (2013).
[26] H. Yu, S. Granville, D. P. Yu, and J.-P. Ansermet, Phys. Rev. Lett. **104**, 146601 (2010).
[27] L. Gravier, S. Serrano-Guisan, F. Reuse, and J.-P. Ansermet, Phys. Rev. B **73**, 024419 (2006).

[28] K. Uchida, M. Ishida, T. Kikkawa, A. Kirihara, T. Murakami, and E. Saitoh, J. Phys.: Condens. Matter **26**, 343202 (2014).
[29] D. Qu, S. Y. Huang, J. Hu, R. Wu, and C. L. Chien, Phys. Rev. Lett. **110**, 067206 (2013).
[30] M. Weiler, M. Althammer, F. D. Czeschka, H. Huebl, M. S. Wagner, M. Opel, I.-M. Imort, G. Reiss, A. Thomas, R. Gross, and S. T. B. Goennenwein, Phys. Rev. Lett. **108**, 106602 (2012).
[31] J. Flipse, F. L. Bakker, A. Slachter, F. K. Dejene, and B. J. van Wees, Nat. Nanotechnol. **7**, 166 (2012).
[32] A. Slachter, F. L. Bakker, J.-P. Adam, and B. J. van Wees, Nat. Phys. **6**, 879 (2010).
[33] R. Sultan, A. D. Avery, J. M. Underwood, S. J. Mason, D. Bassett, and B. L. Zink, Phys. Rev. B **87**, 214305 (2013).
[34] B. L. Zink, A. D. Avery, R. Sultan, D. Bassett, and M. R. Pufall, Solid State Commun. **150**, 514 (2010).
[35] P. Krzysteczko, X. Hu, N. Liebing, S. Sievers, and H. W. Schumacher, Phys. Rev. B **92**, 140405(R) (2015).
[36] M. V. Costache, G. Bridoux, I. Neumann, and S. O. Valenzuela, Nat. Mater. **11**, 199 (2012).
[37] A. D. Avery, M. R. Pufall, and B. L. Zink, Phys. Rev. B **86**, 184408 (2012).
[38] A. D. Avery, M. R. Pufall, and B. L. Zink, Phys. Rev. Lett. **109**, 196602 (2012).
[39] A. Slachter, F. L. Bakker, and B. J. van Wees, Phys. Rev. B **84**, 020412 (2011).
[40] F. L. Bakker, A. Slachter, J.-P. Adam, and B. J. van Wees, Phys. Rev. Lett. **105**, 136601 (2010).
[41] R. E. B. Makinson, Math. Proc. Cambridge Philos. Soc. **34**, 474 (1938).
[42] N. T. Eigenfeld, J. C. Gertsch, G. D. Skidmore, S. M. George, and V. M. Bright, Nanoscale **7**, 17923 (2015).
[43] H. Wang, J. Liu, X. Zhang, and K. Takahashi, Int. J. Heat Mass Transfer **66**, 585 (2013).
[44] H.-D. Wang, J.-H. Liu, X. Zhang, Z.-Y. Guo, and K. Takahashi, Heat Mass Transfer **47**, 893 (2011).
[45] R. Xia, J. L. Wang, R. Wang, X. Li, X. Zhang, X.-Q. Feng, and Y. Ding, Nanotechnology **21**, 085703 (2010).
[46] Q. G. Zhang, B. Y. Cao, X. Zhang, M. Fujii, and K. Takahashi, Phys. Rev. B **74**, 134109 (2006).
[47] R. Berman, *Thermal Conduction in Solids* (Clarendon Press, Oxford, 1976).
[48] D. Y. Petrovykh, K. N. Altmann, H. Höchst, M. Laubscher, S. Maat, G. J. Mankey, and F. J. Himpsel, Appl. Phys. Lett. **73**, 3459 (1998).
[49] G. R. Stewart, Rev. Sci. Instrum. **54**, 1 (1983).
[50] E. H. Sondheimer, Adv. Phys. **1**, 1 (1952).
[51] A. F. Mayadas and M. Shatzkes, Phys. Rev. B **1**, 1382 (1970).
[52] C. R. Pichard, C. R. Tellier, and A. J. Tosser, J. Phys. F: Met. Phys. **10**, 2009 (1980).
[53] O. P. Gupta, J. Phys. F: Met. Phys. **14**, 2899 (1984).
[54] C. Y. Ho, R. W. Powell, and P. E. Liley, J. Phys. Chem. Ref. Data **3**, I (1974).
[55] P. B. Allen, in *Quantum Theory of Real Materials*, edited by J. R. Chelikowsky and S. G. Louie (Kluwer Academic Publishers, Boston, 1996), pp. 219–250.
[56] A. Bid, A. Bora, and A. K. Raychaudhuri, Phys. Rev. B **74**, 035426 (2006).
[57] A. Kapoor, J. A. Rowlands, and S. B. Woods, Phys. Rev. B **9**, 1223 (1974).
[58] M. A. Mitchell, P. G. Klemens, and C. A. Reynolds, Phys. Rev. B **3**, 1119 (1971).
[59] P. Lindenfeld and W. B. Pennebaker, Phys. Rev. **127**, 1881 (1962).
[60] W. R. G. Kemp, P. G. Klemens, and R. J. Tainsh, Philos. Mag. (1798–1977) **4**, 845 (1959).
[61] B. Revaz, M. C. Cyrille, B. L. Zink, I. K. Schuller, and F. Hellman, Phys. Rev. B **65**, 094417 (2002).
[62] B. Fultz, C. C. Ahn, E. E. Alp, W. Sturhahn, and T. S. Toellner, Phys. Rev. Lett. **79**, 937 (1997).
[63] R. Röhlsberger, W. Sturhahn, T. S. Toellner, K. W. Quast, P. Hession, M. Hu, J. Sutter, and E. E. Alp, J. Appl. Phys. **86**, 584 (1999).
[64] H. Frase, B. Fultz, and J. L. Robertson, Phys. Rev. B **57**, 898 (1998).
[65] R. Mazitov, V. Semenov, Y. Lebedev, R. Mulyukov, G. Raab, E. Yadrovskii, and V. Danilenko, JETP Lett. **92**, 238 (2010).
[66] D. R. Queen and F. Hellman, Rev. Sci. Instrum. **80**, 063901 (2009).
[67] C. Y. Ho, M. W. Ackerman, K. Y. Wu, S. G. Oh, and T. N. Havill, J. Phys. Chem. Ref. Data **7**, 959 (1978).
[68] J. P. Moore, T. G. Kollie, R. S. Graves, and D. L. McElroy, J. Appl. Phys. **42**, 3114 (1971).